Environmental Science Nano

Predicting Adsorption of Organic Pollutants on Boron Nitride Nanosheets via in silico Techniques: DFT Computations and QSAR Modeling

Journal:	*Environmental Science: Nano*
Manuscript ID	EN-ART-11-2020-001145.R1
Article Type:	Paper

Predicting Adsorption of Organic Pollutants on Boron Nitride Nanosheets via *in silico* Techniques: DFT Computations and QSAR Modeling

Ya Wang,[†] Weihao Tang,[‡] Yue Peng,[†,*] Zhongfang Chen,[§,*] Jingwen Chen,[‡,*] Zijun Xiao,[‡] Xiaoguang Zhao,[∥] Yakun Qu,[∥] Junhua Li[†]

[†] State Key Joint Laboratory of Environment Simulation and Pollution Control, School of Environment, Tsinghua University, Beijing 100084, China

[‡] Key Laboratory of Industrial Ecology and Environmental Engineering (MOE), School of Environmental Science and Technology, Dalian University of Technology, Linggong Road 2, Dalian 116024, China

[§] Department of Chemistry, University of Puerto Rico, San Juan, PR 00931, USA

[∥] SINOPEC Research Institute of Petroleum Processing (RIPP), Beijing 100083, China

Environmental significance

Superior physical chemical properties for boron nitride nanomaterials endow them with diverse promising applications in different fields. However, their applications as boron nitride adsorbents in removing organic pollutants from the environment is at a nascent stage. Investigating adsorption behaviors for organic pollutants onto boron nitride nanomaterials and developing prediction models to obtain the adsorption data efficiently are crucial for designing novel adsorbents and extending their applications in the environment. Herein DFT computations were utilized for investigating the adsorption of 28 organic compounds onto the boron nitride nanosheet in both gaseous and aqueous environments. Furthermore, four QSAR models for predicting adsorption equilibrium constant values were established, which can serve as efficient tools for high-throughput screening of effective sorbents only *via* clicking a mouse.

Predicting Adsorption of Organic Pollutants on Boron Nitride Nanosheets via *in silico* Techniques: DFT Computations and QSAR Modeling

Ya Wang,[†] Weihao Tang,[‡] Yue Peng,[†,*] Zhongfang Chen,[§,*] Jingwen Chen,[‡,*] Zijun Xiao,[‡] Xiaoguang Zhao,[‖] Yakun Qu,[‖] Junhua Li[†]

[†] State Key Joint Laboratory of Environment Simulation and Pollution Control, School of Environment, Tsinghua University, Beijing 100084, China

[‡] Key Laboratory of Industrial Ecology and Environmental Engineering (MOE), School of Environmental Science and Technology, Dalian University of Technology, Linggong Road 2, Dalian 116024, China

[§] Department of Chemistry, University of Puerto Rico, San Juan, PR 00931, USA

[‖] SINOPEC Research Institute of Petroleum Processing (RIPP), Beijing 100083, China

Abstract

Investigating the adsorption of organic pollutants onto boron nitride nanosheets is crucial for designing novel boron nitride absorbents so as to remove pollutants from the environment. In this study, we performed density functional theory (DFT) computations to investigate the adsorption of 28 aromatic compounds onto boron nitride nanosheets, and developed four quantitative structure-activity relationships (QSARs) models for predicting the logarithm of the adsorption equilibrium constant (log*K*) values of organic pollutants adsorbed onto boron nitride nanosheets in both gaseous and aqueous environments. The DFT-predicted adsorption energies showed that boron nitride nanosheets exhibit stronger adsorption capability than graphene. Our QSAR analyses revealed that van der Waals interactions play dominant roles in the gaseous adsorption, while van der Waals and hydrophobic interactions, are the main driving forces in the aqueous adsorption. This work demonstrates that *in silico* QSAR models can serve as efficient tools for high-throughput prediction of log*K* values for organic pollutants onto boron nitride nanomaterials.

1. Introduction

To date, more than 350,000 chemicals and their mixtures being registered have been produced and utilized,[1] and new chemical products are entering the market with the rate of 12 000 per day.[2] These chemicals will be inevitably released into environment during their lifecycle and become potential environmental pollutants, which give rise to adverse effects on human beings and the environment. Removing these pollutants from the environment is very important for protecting the health of ecosystems. Adsorption, due to its convenient operation, high efficiency, and low-energy consumption, has been extensively applied for eliminating or reducing pollutants from the environment.[3-9] The hexagonal boron nitride nanosheet, as an analogue for graphene, has shown great potential in separating contaminants from the environment by adsorption due to its high specific surface area and chemical stability.[10-13] Therefore, exploring the adsorption for pollutants onto boron nitride nanomaterials is of great significance to develop novel boron nitride-based adsorbent materials for removing contaminants.

Previous experimental studies indicated that boron nitride nanomaterials have good adsorption capabilities towards various species such as metal ions, dyes, and organic solvents.[3,7,14,15] Moreover, different adsorption mechanisms, e.g., van der Waals forces, π-π stacking and electrostatic interactions, may exist simultaneously during the adsorption processes. However, the adsorption behavior of many organic pollutants, especially emerging pollutants (e.g., phthalate ester), onto boron nitride nanomaterials is still unclear, and the adsorption mechanism is not well understood.

Modern computational techniques render us an alternative method to investigate the

adsorption behaviors, which is more efficient than conventional experiments and can provide an atomic level of understanding.[16-20] Considering the large quantities of environmental contaminants, simulating their adsorption behavior towards boron nitride one by one is daunting, time-consuming, and costly, if not impossible. Therefore, it is essential to develop predictive models to obtain the adsorption data on boron nitride nanomaterials.

Very recent studies demonstrated the powerful ability of quantitative structure-activity relationships (QSAR) in predicting the adsorption of organic pollutants on carbon nanomaterials.[18,21-25] In these QSAR models, the most important input parameters are the Abraham descriptors for polyparameter linear free energy relationships (pp-LFERs), which are determined experimentally, and the descriptors characterizing the molecular structures, which can be obtained by theoretical calculations. However, no QSAR model has been proposed to predict the adsorption of organic pollutants onto boron nitride nanomaterials so far.

In this work, we theoretically investigated the adsorption of 28 different aromatic compounds (including phthalate esters) on boron nitride nanosheets in both gaseous and aqueous phases by means of density functional theory (DFT) computations. Based on the DFT computational results, the logarithm of adsorption equilibrium coefficient (log$K$) were estimated. In combination with Abraham descriptors for these 28 compounds, we established pp-LFER models for gaseous and aqueous phases, and evaluated the contributions from different adsorption mechanisms. Furthermore, by utilizing the theoretical molecular structure descriptors, we developed two QSAR models which can predict the adsorption for emerging pollutants in application domain (AD) whose Abraham descriptors are not available. The QSAR models established in this study not only can offer insights into the adsorption

mechanisms for boron nitride nanomaterials, but also lay a foundation for further development of theoretical prediction models to estimate adsorptions onto boron nitride nanomaterials.

2. Computational details

2.1. Organic compounds and boron nitride nanosheets

Herein, 28 aromatic compounds (Table 1) with diverse functional groups, i.e., -NO_2, -CH_3, -OH, -NH_2, -CH_2OH, -CH_2CH_3, -$C(O)CH_3$, -CH_2CH_2OH, -$C(O)OCH_3$, -$OC(O)CH_3$, -$CH_2CH_2CH_3$, -$C(O)OCH_2CH_3$ and -C_6H_5, are used as adsorbate models; the boron nitride nanosheet with supercell size of 8 × 8 × 1 (containing 64 boron atoms and 64 nitrogen atoms) is employed as the adsorbent model.

Table 1. Organic Compounds and Estimated Logarithm Values for Adsorption Equilibrium Coefficient (log*K*) from Our DFT Computations in Gaseous and Aqueous Environments

No.	Compound	Substituents	log*K* (DFT)	
			Gaseous phase	Aqueous phase
1	benzene		2.50	1.61
2	nitrobenzene	$-NO_2$	3.31	3.81
3	toluene	$-CH_3$	4.35	5.04
4	phenol	-OH	5.06	1.47
5	aniline	$-NH_2$	4.44	2.45
6	1,3-dinitrobenzene	$-NO_2$	5.11	3.70
7	4-nitrotoluene	$-NO_2$, $-CH_3$	5.32	4.54
8	2, 4-dinitrotoluene	$-NO_2$, $-CH_3$	8.90	7.42
9	anthracene		11.43	13.69
10	pyrene		12.04	13.95
11	biphenyl		11.00	7.76
12	3,5-dimethylphenol	$-CH_3$, -OH	9.22	6.01
13	ethylbenzoate	$-C(O)OCH_2CH_3$	8.77	7.55
14	4-ethylphenol	$-CH_2CH_3$, -OH	7.28	6.03
15	methylbenzoate	$-C(O)OCH_3$	6.88	5.66
16	(3-methylphenyl)methanol	$-CH_3$, $-CH_2OH$	6.11	4.68
17	1-methylnaphthalene	$-CH_3$	9.66	9.04
18	phenylacetate	$-OC(O)CH_3$	4.44	1.95
19	2-phenylethanol	$-CH_2CH_2OH$	5.28	5.03
20	phenylmethanol	$-CH_2OH$	3.71	3.85
21	propylbenzene	$-CH_2CH_2CH_3$	9.10	4.68
22	p-xylene	$-CH_3$	6.17	4.34
23	dimethyl phthalate (DMP)	$-C(O)OCH_3$	8.27	6.18
24	diethyl phthalate (DEP)	$-C(O)OCH_2CH_3$	10.51	9.71
25	acetophenone	$-C(O)CH_3$	5.47	2.83
26	naphthalene		7.36	6.34
27	1,2-dinitrobenzene	$-NO_2$	5.13	4.69
28	phenanthrene		11.14	11.55

2.2. Density functional theory computations

All the computations were performed in the frame of density functional theory (DFT) by DMol^3 program.[26,27] The Perdew-Burke-Ernzerhof (PBE) functional within the generalized gradient approximation was employed to describe the exchange and correlation potentials.[28] The chosen basis set was double-numerical basis with polarization functions (DNP),[29,30] which is comparable to Gaussian 6-31G(d, p).[31] Besides, the PBE+D2 method with the Grimme van der Waals (vdW) correction[32] was used for describing the long-range electrostatic interactions. A 4×4×1 Monkhorst-pack *k*-point mesh was utilized, and a Methfessel-Paxton smearing of 0.005 Ha[33] was employed for the Brillouin-zone integration. The popular conductor-like screening model (COSMO)[34] with the dielectric constant (78.54) for water was used to implicitly simulate the aqueous environment. COSMO is superior to many other solvent reaction field methods. In this model, the surface charges of a cavity having the same shape of the solute molecule, which describe the electrostatic interactions between the solvent and solute, are determined with the electrostatic potentials directly.[35]

In order to simulate the adsorption onto a boron nitride nanosheet, first the adsorbate models (28 aromatic compounds) and the adsorbent model (a BN nanosheet) were optimized respectively. Afterwards, the global minimum sorbate locations for the 28 complex systems (each including one compound adsorbed on the BN nanosheet) were searched by using Sorption module of Materials Studio 8.0. The most stable configurations being obtained were further optimized with the aforementioned DFT method.

2.3. Estimation for adsorption equilibrium coefficient (*K*)

The changes of Gibbs free energy (ΔG) during the adsorption process can be estimated from the changes of total energy (ΔE), zero point energy (ΔZPE), and entropy (ΔS) following

the equation:

$$\Delta G = \Delta E + \Delta ZPE - T\Delta S \quad (1)$$

where T is temperature, and T = 298.15 K is used for all the calculations. ΔE is also the adsorption energy of a specific adsorbate on the BN nanosheet. ΔE, ΔZPE and ΔS can be obtained by the following equations:

$$\Delta E = E_{BN+X} - E_X - E_{BN} \quad (2)$$

$$\Delta ZPE = ZPE_{BN+X} - ZPE_X - ZPE_{BN} \quad (3)$$

$$\Delta S = S_{BN+X} - S_X - S_{BN} \quad (4)$$

where the subscript BN stands for the boron nitride nanosheet, X represents the adsorbate, while BN+X denotes the complex system including the boron nitride nanosheet and the adsorbed compound. The total energies (E_{BN+X}, E_X and E_{BN}), zero-point energies (ZPE_{BN+X}, ZPE_X and ZPE_{BN}), and entropies (S_{BN+X}, S_X and S_{BN}) were obtained by DFT computations.

We further calculated the adsorption equilibrium coefficient (K) with ΔG.

$$K = e^{-\frac{\Delta G}{RT}} \quad (5)$$

where K is unitless; R is the universal gas constant, i.e., 8.314 $J \cdot mol^{-1} \cdot K^{-1}$. The calculated K is equivalent to the experimentally determined K, which is defined as

$$K = q_e/C_e \quad (6)$$

where q_e represents the equilibrium concentration of the compounds on boron nitride nanosheets; C_e denotes the equilibrium concentration of the compounds in the aqueous/gaseous environments.

2.4. Molecular structure descriptors

Note that the adsorption of organic pollutants on boron nitride nanomaterials is assumed

to be governed by different specific and nonspecific interactions.[3,36] Abraham descriptors can characterize these diverse molecular interactions, and are widely utilized in pp-LFERs, which have the following forms (Eq 7 is used for the partitioning within two condensed phases; while Eq 8 is applied for the partitioning between condensed and gas phases.),[37-42]

$$\log K = eE + sS + aA + bB + vV + c \quad (7)$$

$$\log K = eE + sS + aA + bB + lL + c \quad (8)$$

where K stands for partition coefficient; the uppercase letters, E, S, A, B, V and L, denote the Abraham descriptors; the lowercase letters, e, s, a, b, v and l, are fitting coefficients and c is the regression constant. E is excess molar refraction. V represents McGowan's molar volume [$(cm^3\ mol^{-1})/100$]. L is the logarithmic hexadecane-air partition coefficient. eE represents the interactions which arise through the presence of π- or n-electrons in the compound.[44,45] vV and lL describe the dispersion interactions and cavity formation.[46] Polar interactions are characterized by aA, bB and sS. A refers to hydrogen donor ability, while B denotes hydrogen acceptor ability. S represents dipolarity/polarizability for absorbates. All the Abraham descriptor values for the adsorbates in this study were obtained from the LSER Dataset for CompTox users in the UFZ-LSER database.[47]

The three dimensional (3D) molecular structures for the 28 compounds were obtained by geometry optimization by DFT, and confirmed to be the local minima by frequency analyses. With these optimized molecular structures, we obtained 4885 theoretical molecular structure descriptor values by using the Dragon software (Ver. 6.0).[48] After deleting the descriptors with constant and near-constant values, and selecting the descriptors charactering the property for molecules which may influence the adsorption, we chose 108 theoretical descriptors to

establish QSAR models.

2.5. QSAR models development and evaluation

These 28 compounds were randomly split into a training set consisting of 24 compounds and a validation set including 4 compounds. Based on the log*K* values of DFT calculations and the molecular structure descriptor values for the training set, we utilized the multiple linear regression (MLR) analysis in the SPSS (SPSS 22.0) software package to build up QSAR models, including pp-LFERs models for which Abraham descriptors are as input variables and the models for which Dragon descriptors are input variables. Furthermore, the determination coefficient (R^2), root mean square error for the training set ($RMSE_t$) and for the validation set ($RMSE_v$), leave-one-out cross-validated Q^2 (Q^2_{LOO}) and external explained variance (Q^2_V), were calculated for assessing the goodness of fit, robustness, and prediction ability of QSAR models. Moreover, the application domain (AD) for the predictive models were characterized by Williams plots using standardized residuals (δ^*) and leverage values (h_i).[49]

3. Results and discussion

3.1. log*K* values of DFT calculations and adsorption energies on boron nitride nanosheets

Table 1 lists the log*K* values of 28 aromatic compounds adsorbed on BN nanosheets in the gaseous and aqueous environments predicted by our DFT computations. The predicted log*K* value of benzene on the boron nitride nanosheet in the gaseous phase is 2.50, which is comparable with the experimentally measured value 2.88.[50] We also estimated the log*K* value of nitrobenzene onto graphene in the aqueous phase for which the experimental value is available, and found that the predicted value (4.96) is in good agreement with the experimental one (5.31).[51] These comparisons show that DFT computations can well reproduce the

experimental adsorption data, and can be used to obtain adsorption data when the experimental values are not available.

In addition, all the optimized equilibrium configurations are summarized in Table S1 (Supporting Information, SI). The benzene rings for the 28 organic compounds are all parallel to the boron nitride nanosheet (Table S1). The distances between the mass center of these molecules and the BN nanosheet plane are in the range of 3.168 ~ 3.680 Å, implying the existence of van der Waals interactions. Besides, we performed Hirshfeld population analysis for each compound adsorption on BN nanosheet (Table S2), and the small charge transfer (-0.064 ~ 0.016 e in gaseous phase and -0.096 ~ 0.023 e in aqueous phase) from the compound to the BN nanosheet also indicates physisorption.

We further compared the adsorption energies of 18 different organic compounds onto BN nanosheets with the corresponding values on graphene, in order to examine the differences of adsorption capability between boron nitride and carbon nanomaterials. As shown in Table 2 and Figure 1, the adsorption energies for these 18 aromatic compounds on BN nanosheets are stronger than those on graphene both in gaseous and aqueous environments, and the adsorption energies on graphene correlate with those on the boron nitride nanosheet significantly (Figure 1). Based on these DFT results, the boron nitride nanosheet possibly performs better than graphene in removing contaminants by adsorption.

Table 2. Adsorption Energies (Δ*E*) for 18 Aromatic Compounds on Boron Nitride Nanosheet and Graphene in the Gaseous and Aqueous Environments

No.	Name	Gaseous		Aqueous	
		Δ*E*_BN (kcal/mol)	Δ*E*_G^{24} (kcal/mol)	Δ*E*_BN (kcal/mol)	Δ*E*_G^{24} (kcal/mol)
1	benzene	−17.1	−12.9	−15.9	−11.8
2	nitrobenzene	−21.2	−16.2	−19.7	−14.3
3	toluene	−19.2	−15.3	−19.2	−13.0
4	phenol	−19.2	−14.5	−16.6	−12.4
5	aniline	−21.2	−14.9	−18.1	−12.0
6	phenylmethanol	−19.4	−15.4	−19.8	−14.1
7	phenylacetate	−20.8	−15.5	−18.2	−12.5
8	methylbenzoate	−24.4	−19.3	−22.5	−17.0
9	ethylbenzoate	−27.2	−21.3	−25.0	−18.8
10	acetophenone	−23.8	−18.5	−20.9	−15.6
11	1,3-dinitrobenzene	−24.1	−20.0	−21.5	−17.5
12	1,2-dinitrobenzene	−22.4	−17.6	−20.5	−15.4
13	4-nitrotoluene	−23.9	−19.5	−22.8	−17.5
14	biphenyl	−29.3	−22.0	−26.6	−20.7
15	naphthalene	−25.0	−18.8	−23.9	−18.0
16	phenanthrene	−32.9	−26.6	−31.3	−25.1
17	anthracene	−33.1	−26.9	−32.7	−25.3
18	pyrene	−36.0	−30.5	−35.1	−27.0

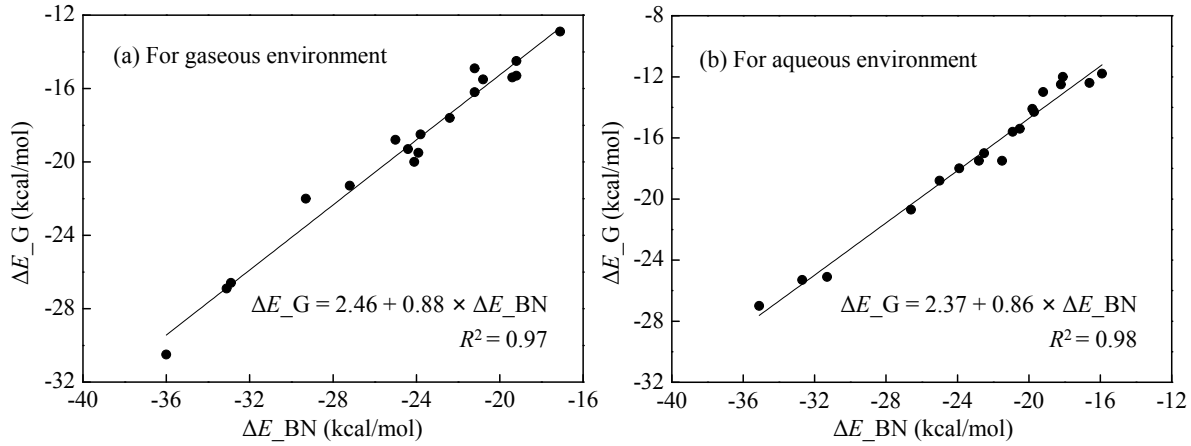

Figure 1. Adsorption energies on graphene (Δ*E*_G) versus those on the boron nitride nanosheet (Δ*E*_BN) by DFT calculations

3.2. QSAR models with Abraham descriptors for log*K* values on boron nitride

Based on Abraham descriptors for the 28 organic compounds, we built up and validated the following pp-LFER predictive models,

for gaseous environment,

$$\log K = -2.508 - 2.352 \times E - 5.510 \times S + 2.509 \times A - 4.252 \times B + 3.670 \times L \quad (9)$$

$$n_t = 24,\ R^2 = 0.89,\ RMSE_t = 0.89,\ F = 29.73,\ p < 0.001,$$
$$n_v = 4,\ Q^2_{LOO} = 0.89,\ Q^2_V = 0.99,\ RMSE_V = 1.88$$

for aqueous environment,

$$\log K = -5.578 + 3.135 \times E - 2.184 \times S + 0.673 \times A - 1.431 \times B + 9.879 \times V \quad (10)$$

$$n_t = 24,\ R^2 = 0.90,\ RMSE_t = 0.99,\ F = 34.12,\ p < 0.001,$$
$$n_v = 4,\ Q^2_{LOO} = 0.83,\ Q^2_V = 0.94,\ RMSE_V = 0.80$$

where n_t is the number of compounds in the training set, and n_v denotes the number of compounds in the validation set. The values for R^2, Q^2_V, Q^2_{LOO}, $RMSE_t$ and $RMSE_V$ imply that these two pp-LFER models have satisfactory goodness of fit, robustness and prediction ability, as they comply with the criteria ($R^2 > 0.60$ and $Q^2 > 0.50$) proposed by Golbraikh *et al*. [52]

Figure 2 shows that the predicted log*K* values from pp-LFER models agree well with the calculated log*K* values *via* DFT method. Note that for the emerging pollutants phthalate esters, i.e., DMP and DEP in current study, their predicted log*K* values [8.00 (DMP_gaseous), 6.97 (DMP_aqueous), 11.48 (DEP_gaseous) and 9.57 (DEP_aqueous)] from pp-LFER models are also comparable with the calculated ones [8.27 (DMP_gaseous), 6.18 (DMP_aqueous), 10.51 (DEP_gaseous) and 9.71 (DEP_aqueous)] from DFT computational results. In terms of the application of the two pp-LFER models, besides four compounds in the vadidation set (i.e., acetophenone, naphthalene, 1, 2-dinitrobenzene, and phenanthrene), we also predicted the log*K* value for a compound outside the dataset, namely fluorene. The predicted log*K* values from models are comparable with those estimated with DFT method (Table S3). All of these demonstrate that these two pp-LFER models can effectively offer adsorption data for organic pollutants including phthalate esters towards boron nitride nanosheets in both gaseous and aqueous environments, and thus can serve as a high-throughput prediction tool.

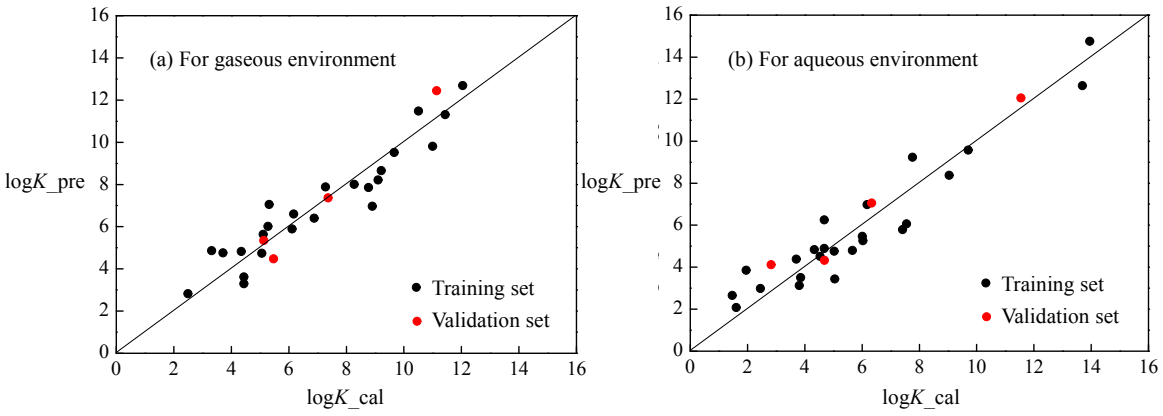

Figure 2. Predicted log*K* values with pp-LFER models ($\log K_{\_pre}$) versus those calculated by DFT method ($\log K_{\_cal}$)

As displayed in Figure S1, all the standardized residuals for the compounds in training set comply with the criteria $|\delta^*| < 3$, indicating that there are no outliers. These two pp-LFER

models (eq 9 and eq 10) can predict the adsorption towards boron nitride nanosheets for diverse organic compounds, i.e., benzene, phenols, nitrobenzenes, alkylbenzenes, anilines, alcohols, esters, ketones, biphenyls and polycyclic aromatic hydrocarbons (PAHs). In terms of the functional groups, the application domain covers various compounds with different functional groups including -NO_2, -CH_3, -OH, -NH_2, -CH_2OH, -CH_2CH_3, -$OC(O)CH_3$, -$C(O)CH_3$, -$C(O)OCH_3$, -CH_2CH_2OH, -$CH_2CH_2CH_3$ and -$C(O)OCH_2CH_3$. When a compound is outside the application domain of the developed models, its prediction is unreliable.

3.3. QSAR models with Dragon descriptors for log*K* values on boron nitride

Note that Abraham descriptors values depend on experimental determinations, and the number for compounds having Abraham descriptors values is ca. 3700.[47] For some of the organic compounds lacking Abraham descriptors values, if they locate in the application domain of the previous models,[53,54] their Abraham descriptors values can be estimated. However, the accuracy of the predicted descriptors values is inferior to those derived from experimental data. While for many organic compounds outside the application domain, the predicted Abraham descriptors values for these compounds are unreliable. Therefore, it is of great importance for developing QSAR models with only the theoretical molecular structure descriptors which can be calculated by computational software directly.

Herein, the optimal QSAR models with Dragon descriptors for predicting the adsorption of organic compounds onto boron nitride nanosheets were developed:

for gaseous environment,

$$\log K = -6.950 + 1.318 \times Sv + 1.323 \times nArOH - 2.058 \times B05[C\text{-}O] - 0.365 \times F05[C\text{-}C] \quad (11)$$

$$n_t = 24,\ R^2 = 0.91,\ RMSE_t = 0.82,\ F = 47.175,\ p < 0.001,$$
$$n_v = 4,\ Q^2_{LOO} = 0.87,\ Q^2_V = 0.94,\ RMSE_V = 0.72$$

for aqueous environment,

$$\log K = -2.788 + 1.247 \times nC - 2.210 \times NRS + 1.193 \times nArNO_2 - 1.009 \times H\text{-}051 \quad (12)$$

$$n_t = 24,\ R^2 = 0.93,\ RMSE_t = 0.88,\ F = 58.75,\ p < 0.001,$$
$$n_v = 4,\ Q^2_{LOO} = 0.82,\ Q^2_V = 0.98,\ RMSE_V = 0.85$$

Likewise, these two QSAR models with $R^2 > 0.60$ and Q^2 (Q^2_{LOO} and Q^2_V) > 0.50, have high goodness of fit, robustness and prediction ability. All the values of variable inflation factors (*VIF*) for the descriptors utilized in eq 10 and eq 11 are less than 10, which implies that there is no serious multi-collinearity among these variables.[55]

As shown in Figure 3, the predicted log*K* values by the QSAR models with Dragon descriptors (eq 11 and eq 12) are in good agreement with those from DFT estimation. For the gaseous phase, in comparison with the pp-LFER model (eq 9), the QSAR model (eq 11) has less descriptors and performs better in goodness of fit, robustness and prediction ability. For the aqueous phase, the QSAR model (eq 12) using less descriptors has better goodness of fit, while the pp-LFER model (eq 10) has fewer $RMSE_V$ value and comparable robustness. In terms of the prediction accuracy for the phthalate esters, the pp-LFER models (eq 9 and eq 10) perform better than the QSAR models (eq 11 and eq 12), since the average prediction errors for phthalate esters with pp-LFER models [0.62 (gaseous phase) and 0.47 (aqueous phase)] are less than those with QSAR models [1.12 (gaseous phase) and 0.78 (aqueous phase)]. We also applied these two QSAR models for predicting the log*K* values for fluorene (Table S3). These results showed that the predicted log*K* values for fluorene with the pp-LFER models (eq 9 and eq 10) are closer to those from DFT calculations than those predicted with the QSAR models (eq 11 and eq 12).

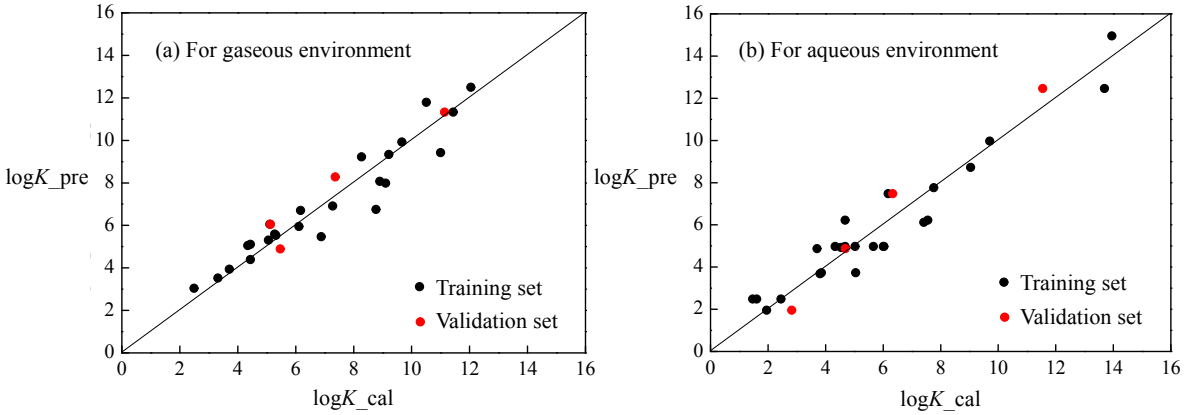

Figure 3. The QSAR predicted log$K$ values with Dragon Descriptors (log$K_{_pre}$) versus those calculated by DFT method (log$K_{_cal}$)

Besides, based on the standardized residuals (δ*) and leverage values (h) for the compounds in the training set, we characterized the application domains (ADs) as illustrated in Figure S2. With the $|\delta^*|$ values less than three, all the compounds are located in the ADs. Note that the h value for 4-ethylphenol (1.0) is larger than the warning leverage value (h*=0.625) while its $|\delta^*|$ value is smaller than 3 (Figure S2b), indicating that its structure is very different from other compounds in the training set and it is influential on the prediction model for aqueous phase. It is known that the application domain for a prediction model depends on the compounds utilized when this model is developed. The established QSAR models (eq 11 and eq 12) with the Dragon descriptors have the same ADs with those for pp-LFERs (eq 9 and eq 10), covering diverse organic compounds. Moreover, the two models (eq 11 and eq 12) can be applied for obtaining log$K$ values of more emerging pollutants lacking pp-LFERs descriptors values.

3.4. Adsorption mechanisms

pp-LFER models. As shown in the developed pp-LFER models (eq 9 and eq 10), for both gaseous and aqueous systems, the five sets of parameters, namely *eE*, *vV*/*lL*, *aA*, *bB* and *sS*, are used, but they have different values, which indicate that the molecular interactions they are describing play different roles in the adsorption (Figure 4).

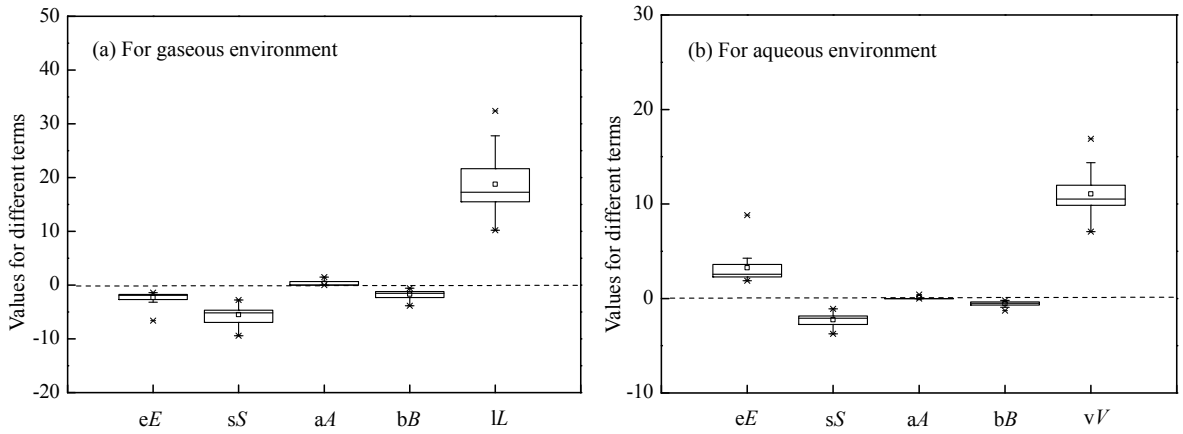

Figure 4. Box and whisker plots for the values of different terms in pp-LFER models. The lines below and above the rectangles in the plot denote the minimum and maximum values for each term; the lines within the rectangles mean the 50th percentiles; the bottom and the top for the rectangles represent the 25th and 75th percentiles.

In terms of the adsorption in the gaseous environment, the term *lL* plays a dominant role as its relative contribution to the adsorption ranges from 53% to 68%. *lL* in eq 8 represents dispersion interactions. Therefore, the dispersion interactions are key driving forces for adsorption on the BN nanosheet in the gaseous phase. The relative contribution to the adsorption for *sS* is in the range of 12% ~ 25%, which is second only to that for *lL*. The term *sS* describes the interactions related to the polarity and polarizability of the adsorbates. Note that the fitting coefficient *s* is negative, implying that the compound having high value of *S* is

not liable to be adsorbed onto boron nitride nanosheets. As shown in eq 9 and Figure 4, the H-bonding interactions between H-donating adsorbate and H-accepting adsorbent, characterized by the term *aA*, do positively contribute (ca. 0 ~ 6%) to the adsorption. While for the H-bonding interactions between H-accepting adsorbate and H-donating adsorbent, being denoted by the term *bB*, its contribution to the adsorption ranges from 2% to 10% negatively. The reason may be that the nitrogen atoms on the boron nitride nanosheet is rich in electrons, which can accept hydrogen atoms from the compounds lacking electrons, thereby increasing the interactions between the compounds and the nanosheet. In addition, the term *eE* representing the interactions related to π or *n*-electron pair has a negative contribution (ranging from 4% to 13%) to the adsorption. It implies that the compound possessing less π or *n* electrons tends to be adsorbed by boron nitride nanomaterials for accepting the electrons.

For the adsorption in the aqueous environment, the term *vV* representing the dispersion and hydrophobic interactions has the most significant influence on the log*K* values with relative contributions ranging from 41% to 59%, which indicates that the dispersion and hydrophobic interactions play vital roles in the adsorption for organic compounds onto the boron nitride nanosheet. The term *eE*, denoting the interactions related to π or *n*-electron pair, has a positive contribution to the adsorption with the relative contribution in the range of 8% ~ 26%. Note that its contribution in the aqueous phase is positive, which is contrary to that in the gaseous phase, most likely the π or *n* electrons from the compound can interact with one hydrogen atom in water molecules, and the other hydrogen atom in water molecules can interact with the nitrogen atoms of boron nitride surface, thereby assisting the adsorption of the compound towards boron nitride nanosheets. Therefore, it seems that the compound having more π or *n*

electrons become liable to be adsorbed towards the boron nitride nanosheet in aqueous phase. s*S* represents the interactions related to the polarity and polarizability of the compounds, and has a negative contribution (ranging from 5% ~ 15%) to the adsorption. Besides, the hydrogen bonding interactions also play roles in the adsorption. The term *aA* describing the H-bonding interactions between H-donating adsorbate and H-accepting system (including adsorbent and water) contributes positively to the adsorption (ranging from 0 ~ 2%), while the term *bB* representing the H-bonding interactions between H-accepting adsorbate and H-donating system contributes negatively to the adsorption (in the range of 1% ~ 5%). The roles for hydrogen donating/accepting abilities in the adsorption on boron nitride nanosheets in the aqueous phase are similar to those in the gaseous phase.

QSAR models with Dragon descriptors. Table 3 lists the predictive variables and their standardized coefficients, *t*, *p* values, and variable inflation factor (*VIF*) for the QSAR models with Dragon descriptors (eq 11 and eq 12). Note that the predictive variables used for the gaseous and aqueous phases are different, which implies that the adsorption mechanisms in the gaseous phase are different from that in the aqueous phase.

For the adsorption in the gaseous phase, as shown in eq 11, the descriptors *Sv*, *nArOH*, *B05[C-O]* and *F05[C-C]* are combined to predict the log*K* values. *Sv*, sum of atomic van der Waals volumes (scaled on carbon atom),[56] has the highest standardized coefficient among these four descriptors (Table 3), indicating that it is the most influential predictive variable for the adsorption onto the boron nitride nanosheet in gaseous environment. It also indicates that van der Waals interactions play an important role in the adsorption, which is in good agreement with the pp-LFER model in gaseous phase. Besides, the descriptor *nArOH* is the number of

aromatic hydroxyls,[57] and its coefficient is positive, which suggests that the compound having a large *nArOH* value tends to be adsorbed onto the boron nitride nanosheet, because the hydrogen atom from the aromatic hydroxyls lacking electrons can be liable to interact with the nitrogen atom possessing rich electrons from boron nitride surface. The descriptors *B05[C-O]*[58] and *F05[C-C]*[59] denote different atom pairs, and both of them have negative coefficients. These two descriptors, to some extent, reflect the spatial structure for the compound. There exists steric hindrance during the adsorption for the compound having large values for *B05[C-O]* or *F05[C-C]*.

Table 3. Description for the Predictive Variables and Their Standardized Coefficients, *t*, *p* Values and Variable Inflation Factor (*VIF*)

Gaseous phase					
Descriptors	Description	Standardized coefficients	*t**	*p**	*VIF*
Sv	Sum of atomic van der Waals volumes (scaled on Carbon atom)	1.403	7.275	< 0.001	7.724
nArOH	number of aromatic hydroxyls	0.161	2.194	< 0.05	1.115
B05[C-O]	Presence/absence of C-O at topological distance 5	–0.377	–4.413	< 0.001	1.513
F05[C-C]	Frequency of C-C at topological distance 5	–0.523	–2.634	< 0.02	8.189
Aqueous phase					
Descriptors	Description	Standardized coefficients	*t**	*p**	*VIF*
nC	number of carbon atoms	1.011	14.572	< 0.001	1.222
NRS	number of ring systems	–0.138	–2.114	< 0.05	1.080
$nArNO_2$	number of nitro groups (aromatic)	0.222	3.296	< 0.01	1.149

H-051	H attached to alpha-C	–0.189	–2.987	< 0.01	1.016

* *t* denotes the statistic from *t*-test; *p* is the significance level of *t*-test.

When the adsorption in the aqueous phase is concerned, as illustrated in eq 12, the descriptors, namely *nC*, *NRS*, $nArNO_2$ and *H-051*, contribute differently to the log*K* values. The standardized coefficients in Table 3 shows that the descriptor *nC* (the number of carbon atoms)[60] is the most influential variable in predicting the log*K* values. The positive coefficient of *nC* indicates that the compound with more carbon atoms tends to be adsorbed on the boron nitride nanosheet. The descriptor $nArNO_2$[61] denoting the number of nitro groups (aromatic) has a positive coefficient, which indicates that when interacting with the boron nitride nanosheet, a compound with more nitro groups (aromatic) will have stronger interactions compared with a compound with less nitro groups (aromatic). This phenomenon can be understood by the electrophilic property of the nitro groups, which tend to withdraw the electrons from the surface of boron nitride, thereby increasing the interactions between the compounds and the boron nitride nanosheet. The descriptor *H-051* is an atom-centered fragment, describing the existence of hydrogen attached to alpha-C.[62] *NRS* characterizes the number of ring systems.[63] The coefficients for *H-051* and *NRS* are both negative, implying that the compound with a lower *H-051* or *NRS* value will be adsorbed by boron nitride nanomaterial more easily.

Furthermore, taking benzene as an example, we computed its adsorption energy onto boron nitride nanosheet without vdW correction, and found that the absolute values for the obtained adsorption energies without vdW corrections (7.2 kcal/mol in gaseous phase and 6.3

kcal/mol in aqueous phase) are ca. 10 kcal/mol less than those (17.1 kcal/mol in gaseous phase and 15.9 kcal/mol in aqueous phase) calculated with PBE+D2 method. It implies that the noncovalent interactions (van der Waals in particular) play significant roles in the adsorption, which is also supported by the non-covalent interactions analysis of the simplified model system (Figure S3).[64]

To summarize, the adsorption mechanisms for organic pollutants onto boron nitride nanosheets in gaseous environment are different from those in aqueous environment. The van der Waals interactions prevail in the gaseous adsorption, while for the aqueous adsorption, the main driving forces are van der Waals and hydrophobic interactions.

4. Conclusions

In this study, DFT computations were successfully utilized to probe the atomic-level details for adsorption of 28 diverse organic compounds onto the boron nitride nanosheet in both gaseous and aqueous environments. Adsorption energies implied that the boron nitride nanosheet has stronger adsorption capability than graphene. Four QSAR models for predicting log*K* values were further established, which can serve as efficient tools for high-throughput screening of effective sorbents. Especially, when the pp-LFER descriptors of organic compounds are not available, the adsorption behavior can still be well predicted by the QSAR models with only theoretical molecular descriptors. Moreover, the developed QSAR models can provide us insights into the mechanisms involved in the adsorption onto boron nitride nanomaterials. These *in silico* techniques, i.e., DFT computations and QSAR modeling, make it possible for us to obtain the adsorption data on boron nitride nanosheets only *via* clicking a mouse, and such techniques can be extended to many other sorbents systems.

Supporting information

Electronic supplementary information (ESI) is available: (1) Adsorption equilibrium configuration (Table S1); (2) Charge transfer between the compound and the boron nitride nanosheet (Table S2); (3) Estimated logarithm values for adsorption equilibrium coefficient (log*K*) for fluorene (Table S3); (4) Williams plots of standardized residuals (δ*) versus leverage values (*h*) for pp-LFER models (Figure S1); (5) Williams plots of standardized residuals (δ*) versus leverage values (*h*) for QSAR models (Figure S2); (6) Non-covalent interactions (NCI) analysis for the interactions between C6H6 and $B_{15}N_{15}H_{14}$ with the Multiwfn program (Figure S3).

Corresponding authors

*Yue Peng - State Key Joint Laboratory of Environment Simulation and Pollution Control, School of Environment, Tsinghua University, Beijing 100084, China; E-mail: pengyue83@tsinghua.edu.cn

* Zhongfang Chen - Department of Chemistry, University of Puerto Rico, San Juan, PR 00931, USA; Email: zhongfangchen@gmail.com

* Jingwen Chen - School of Environmental Science and Technology, Dalian University of Technology, Dalian 116024, China; E-mail: jwchen@dlut.edu.cn.

Author contributions

The manuscript was written through contributions of all authors. All authors have given approval to the final version of the manuscript.

Notes

The authors declare no competing financial interest.

Acknowledgements

The study was supported in China by the National Key Research and Development Program (2018YFC0214100 and 2017YFC0211000) and in USA by NASA (Grant Number 80NSSC19M0236) and the NSF Centre for the Advancement of Wearable Technologies (Grant 1849243).

References

(1) Wang, Z.; Walker, G. W.; Muir, D. C. G.; Nagatani-Yoshida, K. Toward a global understanding of chemical pollution: A first comprehensive analysis of national and regional chemical inventories. *Environ. Sci. Technol.* **2020**, *54* (5), 2575–2584.

(2) Rojas, S.; Horcajada, P. Metal–organic frameworks for the removal of emerging organic contaminants in water. *Chem. Rev.* **2020**, *120* (16), 8378–8415.

(3) Yu, S.; Wang, X.; Pang, H.; Zhang, R.; Song, W.; Fu, D.; Hayat, T.; Wang, X. Boron nitride-based materials for the removal of pollutants from aqueous solutions: A review. *Chem. Eng. J.* **2018**, *333*, 343–360.

(4) Zhao, J.; Wang, Z. Y.; White, J.; Xing, B. S. Graphene in the aquatic environment: Adsorption, dispersion, toxicity and transformation. *Environ. Sci. Technol.* **2014,** *48* (17), 9995–10009.

(5) Xue, Y. M.; Dai, P. C.; Jiang, X. F.; Wang, X. B.; Zhang, C.; Tang, D. M.; Weng, Q. H.; Wang, X.; Pakdel, A.; Tang, C. C.; Bando, Y.; Golberg, D. Template-free synthesis of boron nitride foam-like porous monoliths and their high-end applications in water purification. *J. Mater. Chem. A* **2016**, *4*, 1469–1478.

(6) Lian, G.; Zhang, X.; Zhang, S.; Liu, D.; Cui, D.; Wang, Q. Controlled fabrication of ultrathin-shell BN hollow spheres with excellent performance in hydrogen storage and wastewater treatment. *Energ. Environ. Sci.* **2012**, *5*, 7072–7080.

(7) Liu, D.; Lei, W.; Qin, S.; Klika, K.; Chen, Y. Superior adsorption of pharmaceutical molecules by highly porous BN nanosheets. *Phy. Chem. Chem. Phy.* **2016**, *18*, 84–88.

(8) Jiang, L.; Liu, Y.; Liu, S.; Zeng, G.; Hu, X.; Hu, X.; Guo, Z.; Tan, X.; Wang, L.; Wu, Z. Adsorption of estrogen contaminants by graphene nanomaterials under natural organic matter preloading: Comparison to carbon nanotube, biochar, and activated carbon. *Environ. Sci. Technol.* **2017**, *51* (11), 6352–6359.

(9) Wang, J.; Chen, B.; Xing, B. S. Wrinkles and folds of activated graphene nanosheets as fast and efficient adsorptive sites for hydrophobic organic contaminants. *Environ. Sci. Technol.* **2016**, *50* (7), 3798–3808.

(10) Golberg, D.; Bando, Y.; Huang, Y.; Terao, T.; Mitome, M.; Tang, C. C.; Zhi, C. Y. Boron nitride nanotubes and nanosheets. *ACS Nano* **2010**, *4*, 2979−2993.

(11) Ye, J.; Zhu, X.; Cheng, B.; Yu, J.; Jiang, C. Few-layered graphene-like boron nitride: A highly efficient adsorbent for indoor formaldehyde removal. *Environ. Sci. Technol. Lett.* **2017**, *4* (1), 20–25.

(12) Liu, D.; He, L.; Lei, W.; Klika, K. D.; Kong, L.; Chen, Y. Multifunctional polymer/porous boron nitride nanosheet membranes for superior trapping emulsified oils and organic molecules. *Adv. Mater. Interfaces* **2015**, *2* (12), 1500228.

(13) Lei, W.; Portehault, D.; Liu, D.; Qin, S.; Chen, Y. Porous boron nitride nanosheets for effective water cleaning. *Nat. Commun.* **2013**, *4*, 1777.

(14) Jia, H.; Li, J.; Liu, Z.; Gao, R.; Abbas, S.; Fang, Y.; Yu, C.; Tang, C. Three-dimensional carbon boron nitrides with a broken, hollow, spherical shell for water treatment. *RSC Adv.* **2016**, *6*, 78252–78256.

(15) Kobayashi, H.; Fukuoka, A., Hexagonal boron nitride for adsorption of saccharides. *J. Phys. Chem. C* **2017**, *121* (32), 17332–17338.

(16) Yu, S.; Wang, X.; Yao, W.; Wang, J.; Ji, Y.; Ai, Y.; Alsaedi, A.; Hayat, T.; Wang, X. Macroscopic, spectroscopic, and theoretical investigation for the interaction of phenol and naphthol on reduced graphene oxide. *Environ. Sci. Technol.* **2017**, *51* (6), 3278–3286.

(17) Karlický, F.; Otyepková, E.; Lo, R.; Pitoňák, M.; Jurečka, P.; Pykal, M.; Hobza, P.; Otyepka, M. Adsorption of organic molecules to van der Waals materials: Comparison of fluorographene and fluorographite with graphene and graphite. *J. Chem. Theory Comput.* **2017**, *13* (3), 1328–1340.

(18) Roy, J.; Ghosh, S.; Ojha, P. K.; Roy, K. Predictive quantitative structure–property relationship (QSPR) modeling for adsorption of organic pollutants by carbon nanotubes (CNTs). *Environ. Sci. Nano* **2019**, *6* (1), 224–247.

(19) Comer, J.; Chen, R.; Poblete, H.; Vergara-Jaque, A.; Riviere, J. E. Predicting adsorption

affinities of small molecules on carbon nanotubes using molecular dynamics simulation. *ACS Nano* **2015**, *9* (12), 11761–11774.

(20) Tang, H.; Zhao, Y.; Shan, S. J.; Yang, X. N.; Liu, D. M.; Cui, F. Y.; Xing, B. S. Wrinkle- and edge-adsorption of aromatic compounds on graphene oxide as revealed by atomic force microscopy, molecular dynamics simulation, and density functional theory. *Environ. Sci. Technol.* **2018**, *52* (14), 7689–7697.

(21) Ersan, G.; Apul, O. G.; Karanfil, T. Predictive models for adsorption of organic compounds by Graphene nanosheets: comparison with carbon nanotubes. *Sci. Total Environ.* **2019**, *654*, 28–34.

(22) Apul, O. G.; Wang, Q.; Shao, T.; Rieck, J. R.; Karanfil, T. Predictive model development for adsorption of aromatic contaminants by multi-walled carbon nanotubes. *Environ. Sci. Technol.* **2013**, *47* (5), 2295–2303.

(23) Wang, Y.; Chen, J. W.; Tang, W. H.; Xia, D. M.; Liang, Y. Z.; Li, X. H. Modeling adsorption of organic pollutants onto single-walled carbon nanotubes with theoretical molecular descriptors using MLR and SVM algorithms. *Chemosphere* **2019**, *214*, 79–84.

(24) Wang, Y.; Chen, J. W.; Wei, X. X.; Hernandez Maldonado, A. J.; Chen, Z. F. Unveiling adsorption mechanisms of organic pollutants onto carbon nanomaterials by density functional theory computations and linear free energy relationship modeling. *Environ. Sci. Technol.* **2017**, *51* (20), 11820–11828.

(25) Wang, Y.; Comer, J.; Chen, Z. F.; Chen, J. W.; Gumbart, J. C. Exploring adsorption of neutral aromatic pollutants onto graphene nanomaterials *via* molecular dynamics simulations

and theoretical linear solvation energy relationships. *Environ. Sci. Nano* **2018**, *5* (9), 2117–2128.

(26)Delley, B. An all-electron numerical method for solving the local density functional for polyatomic molecules. *J. Chem. Phys.* **1990**, *92* (1), 508−517.

(27)Delley, B. From molecules to solids with the DMol^3 approach. *J. Chem. Phys.* **2000**, *113* (18), 7756−7764.

(28)Perdew, J. P.; Burke, K.; Ernzerhof, M. Generalized gradient approximation made simple. *Phys. Rev. Lett.* **1996**, *77* (18), 3865−3868.

(29)Benedek, N. A.; Snook, I. K.; Latham, K.; Yarovsky, I. Application of numerical basis sets to hydrogen bonded systems: A density functional theory study. *J. Chem. Phys*. **2005**, *122* (14), 144102−144108.

(30)Inada, Y. and Orita, H. Efficiency of numerical basis sets for predicting the binding energies of hydrogen bonded complexes: Evidence of small basis set superposition error compared to Gaussian basis sets. *J. Comput. Chem*. **2008**, *29* (2), 225−232.

(31)Liu, P. and Rodriguez, J. A. Catalysts for hydrogen evolution from the [NiFe] hydrogenase to the Ni_2P (001) surface: The importance of ensemble effect. *J. Am. Chem. Soc*. **2005**, *127* (42), 14871−14878.

(32)Grimme, S. Semiempirical GGA-type density functional constructed with a long-range dispersion correction. *J. Comput. Chem*. **2006**, *27* (15), 1787−1799.

(33)Wang, H. M.; Wang, H. X.; Chen, Y.; Liu, Y. J.; Zhao, J. X.; Cai, Q. H.; Wang, X. Z. Phosphorus-doped graphene and (8, 0) carbon nanotube: Structural, electronic, magnetic

properties, and chemical reactivity. *Appl. Surf. Sci.* **2013**, *273*, 302−309.

(34)Andzelm, J.; Kölmel, C.; Klamt, A. Incorporation of solvent effects into the density functional calculations of molecular energies and geometries. *J. Chem. Phys.* **1995**, *103* (21), 9312−9320.

(35) Barone, V. and Cossi, M. Quantum calculation of molecular energies and energy gradients in solution by a conductor solvent model. *J. Chem. Phys. A* **1998**, *102* (11), 1995−2001.

(36) Goss, K.; Bronner, G.; Harner, T.; Hertel, M.; Schmidt, T. C. The partition behavior of fluorotelomer alcohols and olefins. *Environ. Sci. Technol.* **2006**, *40* (11), 3572−3577.

(37) Abraham, M. H.; Grellier, P. L.; McGill, R. A. Determination of olive oil-gas and hexadecane-gas partition coefficients, and calculation of the corresponding olive oil-water and hexadecane-water partition coefficients. *J. Chem. Soc., Perkin Trans. 2* **1987**, *6*, 797−803.

(38) Abraham, M. H. and McGowan, J. C. The use of characteristic volumes to measure cavity terms in reversed phase liquid chromatography. *Chromatographia* **1987**, *23* (4), 243−246.

(39) Abraham, M. H.; Whiting, G. S.; Doherty, R. M.; Shuely, W. J. Hydrogen bonding. Part 13. A new method for the characterization of GLC stationary phases-The Laffort data set. *J. Chem. Soc. Perkin Trans. 2* **1990**, 8, 1451−1460.

(40) Abraham, M. H.; Whiting, G. S.; Doherty, R. M.; Shuely, W. J. Hydrogen bonding. XVI. A new solute solvation parameter, π_2^H, from gas chromatographic data. *J. Chromatogr.* **1991**, *587* (2), 213−228.

(41) Abraham, M. H. Hydrogen-bonding. 31. Construction of a scale of solute effective or summation hydrogen-bond basicity. *J. Phys. Org. Chem.* **1993**, *6* (12), 660−684.

(42) Abraham, M. H. Scales of solute hydrogen-bonding: Their construction and application to physicochemical and biochemical processes. *Chem. Soc. Rev.* **1993**, *22* (2), 73−83.

(43) Endo, S.; Goss, K., Predicting partition coefficients of polyfluorinated and organosilicon compounds using polyparameter linear free energy relationships (PP-LFERs). *Environ. Sci. Technol.* **2014**; *48*, 2776-2784.

(44) Abraham, M. H.; Ibrahim, A.; Zissimos, A. M. Determination of sets of solute descriptors from chromatographic measurements. *J. Chromatogr. A* **2004**, *1037* (1-2), 29-47.

(45) Platts, J. A.; Abraham, M. H.; Butina, D.; Hersey, A. Estimation of molecular linear free energy relationship descriptors by a group contribution approach. 2. Prediction of partition coefficients. *J. Chem. Inf. Comput. Sci*. **2000**, *40* (1), 71−80.

(46) Goss, K., et al., The Partition behavior of fluorotelomer alcohols and olefins. *Environ. Sci. Technol*. **2006**, *40* (11), 3572−3577.

(47) Ulrich, N.; Endo, S.; Brown, T. N.; Watanabe, N.; Bronner, G.; Abraham, M. H.; Goss, K.-U. UFZ-LSER database v 3.2.1 [Internet], Leipzig, Germany, Helmholtz Centre for Environmental Research-UFZ. **2017**

(48) Talete srl, 2014. Dragon (Software for Molecular Descriptor Calculation) Version 6.0. http://www.talete.mi.it/.

(49) Gramatica, P. Principles of QSAR models validation: Internal and external. *QSAR Comb. Sci*. **2007**, *26* (5), 694−701.

(50) Li, J.; Xiao, X.; Xu, X.; Lin, J.; Huang, Y.; Xue, Y.; Jin, P.; Zou, J.; Tang, C., Activated boron nitride as an effective adsorbent for metal ions and organic pollutants. *Sci. Rep.* **2013**, *3*,

3208.

(51) X. X. Chen and B. L. Chen, Macroscopic and spectroscopic investigations of the adsorption of nitroaromatic compounds on graphene oxide, reduced graphene oxide, and graphene nanosheets, *Environ. Sci. Technol*., **2015**, *49*, 6181−6189.

(52) Golbraikh, A.; Shen, M.; Xiao, Z. Y.; Xiao, Y. D.; Lee, K. H.; Tropsha, A. Rational selection of training and test sets for the development of validated QSAR models. *J. Comput. Aided Mol. Des*. **2003**, *17*, 241–253.

(53) Brown, T.N. Predicting hexadecane-air equilibrium partition coefficients (*L*) using a group contribution approach constructed from high quality data. *SAR QSAR Environ. Res.* **2014**, *25*(1), 51–71.

(54) Liang, Y.; Xiong, R.; Sandler, S. I.; Di Toro, D. M. Quantum chemically estimated Abraham solute parameters using multiple solvent–water partition coefficients and molecular polarizability. *Environ. Sci. Technol*., **2017**, *51*(17), 9887−9898.

(55) Robinson, C.; Schumacker, R. E. Interaction effects: centering, variance inflation factor, and interpretation issues. *Multiple Linear Regression Viewpoints* **2009**, *35*, 6–11.

(56) Larsson, J.; Gottfries, J.; Muresan, S.; Backlund, A., ChemGPS-NP: Tuned for navigation in biologically relevant chemical space. *J. Nat. Prod*. **2007**, *70* (5), 789−794.

(57) Borhani, T. N. G.; Saniedanesh, M.; Bagheri, M.; Lim, J. S. QSPR prediction of the hydroxyl radical rate constant of water contaminants. *Water Res.* **2016**, *98*, 344−353.

(58) Todeschini, R.; Consonni, V. Handbook of molecular descriptors. **2000**. Wiley-VCH, Weinheim, Germany.

(59) De, P.; Bhattacharyya, D.; Roy, K. Application of multilayered strategy for variable selection in QSAR modeling of PET and SPECT imaging agents as diagnostic agents for Alzheimer's disease. *Struct. Chem.* **2019**, *30* (6), 2429−2445.

(60) Mannhold, R.; Poda, G. I.; Ostermann, C.; Tetko, I. V. Calculation of molecular lipophilicity: State-of-the-art and comparison of log*P* methods on more than 96,000 compounds. *J Pharm. Sci.* **2009**, *98* (3), 861−893.

(61) Papa, E.; Pilutti, P.; Gramatica, P. Prediction of PAH mutagenicity in human cells by QSAR classification. *SAR QSAR Environ. Res.* **2008**, *19* (1-2), 115−127.

(62) Fernández, A.; Rallo, R.; Giralt, F. Prioritization of *in silico* models and molecular descriptors for the assessment of ready biodegradability. *Environ. Res.* **2015**, *142*, 161−168.

(63) Feher, M.; Schmidt, J. M. Property distributions: Differences between drugs, natural products, and molecules from combinatorial chemistry. *J. Chem. Inf. Comp. Sci.* **2002**, *43* (1), 218−227.

(64) Pastorczak, E.; Corminboeuf, C. Perspective: Found in translation: Quantum chemical tools for grasping non-covalent interactions. *J. Chem. Phys*. **2017**, *146* (12), 120901.